Chapter 5

Experimental Analyses into Ultrasonic Vibration-Assisted Grinding of AISI D2 Tool Steel with Alumina Wheel

5 Introduction

This chapter describes experimental studies that were carried out to assess the enhancement in grinding productivity of AISI D2 tool steel by adopting the ultrasonic vibration assisted dry grinding (UVADG) mode. Experimental works were conducted on a UVADG setup that was indigenously developed and manufactured. The grinding productivity in the UVADG mode was assessed by comparing the grinding forces, force ratio, specific grinding energy, surface roughness, bearing area curve (BAC), BAC ratio, ground surface morphology, and topography, grinding temperature, grinding chip morphology, microstructure, and microhardness analysis achieved in conventional dry grinding (CDG) and conventional wet grinding (CWG) modes. The UVADG mode at optimised amplitude and frequency results in lesser grinding forces and better surface integrity than CDG and CWG modes. With UVADG mode, the impact of overlapping induced by ultrasonic vibration resulted in a higher BAC ratio (88.71%) and a steeper BAC. This BAC ratio reflects the ground surface in UVADG mode, which is less susceptible to antifriction and antiwear characteristics than CDG and CWG modes. Besides, small, thin chips generated in UVADG mode indicate the ease of grinding of AISI D2 tool steel. The experimental outcomes revealed that the UVADG mode has a greater potential for improving the grindability of AISI D2 tool steel. The current study also promotes the need for a sustainable grinding method for "difficult to machine" materials adopting UVADG mode.

Moreover, the available literature cited in Chapter 2 revealed that ultrasonic assisted grinding could achieve almost the same decrease in grinding force and ground surface

roughness even when the grinding parameters were substantially different, whereas vibration parameters remained constant. Thus, it is worth addressing whether UVADG mode can consistently provide outstanding performance over such a varied range of grinding and vibration parameters. Therefore, the present research focuses on improving the grinding performance of AISI D2 tool steel by examining the influence of grinding parameters on UVADG mode and comparing it to CDG and CWG modes. The downfeed and vibration amplitude varied throughout the test, while the grinding speed, worktable feed rate, and ultrasonic frequency stayed unchanged. The bearing area curve (BAC) and BAC ratio were computed using the three-dimensional roughness parameters in order to determine the best antifriction and antiwear properties of the ground workpiece. Since the current study correlates to "difficult to machine" materials, namely AISI D2 tool steel, an advantage of UVADG on the grinding forces, force ratio, surface integrity, antifriction, and antiwear characteristics parameters are of importance for engineering applications. These parameters have been established through this work, which is the unique novelty of this present work, and it offers an improvement in our understanding of ultrasonic vibration assisted dry grinding of "difficult to machine" steels, namely AISI D2 tool steel.

5.1 Experimental procedure

The grinding experiments were conducted using a surface grinding machine with an alumina grinding wheel. The details of the experimental procedure have already been discussed in Chapter 3 and Section 3.3. The grinding experimental specifications illustrated in Table 5.1 were adequately taken based on the preliminary experiments.

Table 5.1 Parameters setting for grinding.

Parameters	Conditions
Grinding type	Plunge surface grinding
Grinding modes	Conventional dry grinding (CDG), Conventional wet grinding (CWG), Ultrasonic vibration assisted dry grinding (UVADG)
Cutting fluid	Water based soluble oil (Cimtech-D14)
Grinding wheel specification	AA-60-K-5-V-6
Workpiece material	AISI D2 tool steel
Wheel speed (V_c)	39.42 m/s
Worktable feed rate (V_w)	9 m/min
Downfeed (a_p)	10 – 40 µm
Ultrasonic frequency (f_{ug})	21 kHz
Vibration amplitude (A_{ug})	4 – 10 µm
Dresser	Single point diamond
Dressing down feed	50 µm in 8 passes
Dressing feed	180 mm per min

5.2 Result and discussion

5.2.1 Grinding forces

In the grinding domain, grinding force is a critical parameter to characterize the grinding process because it helps estimate the grinding force ratio, grinding wheel life, surface roughness, and grinding temperature [265]. Figure 5.1 (a, b) depicts the change of tangential (F_t) and normal (F_n) grinding force computed during each pass for CDG, CWG

and UVADG (at A_{ug} = 4, 7, and 10 µm) modes at 10 µm and 40 µm downfeed. Each set of experiments in this investigation follows the same pattern. As shown in Figure 5.1 (a, b), owing to the expected interaction of mostly negatively raked abrasives present in the abrasive wheel's edge, normal grinding force components are always higher than the tangential grinding force.

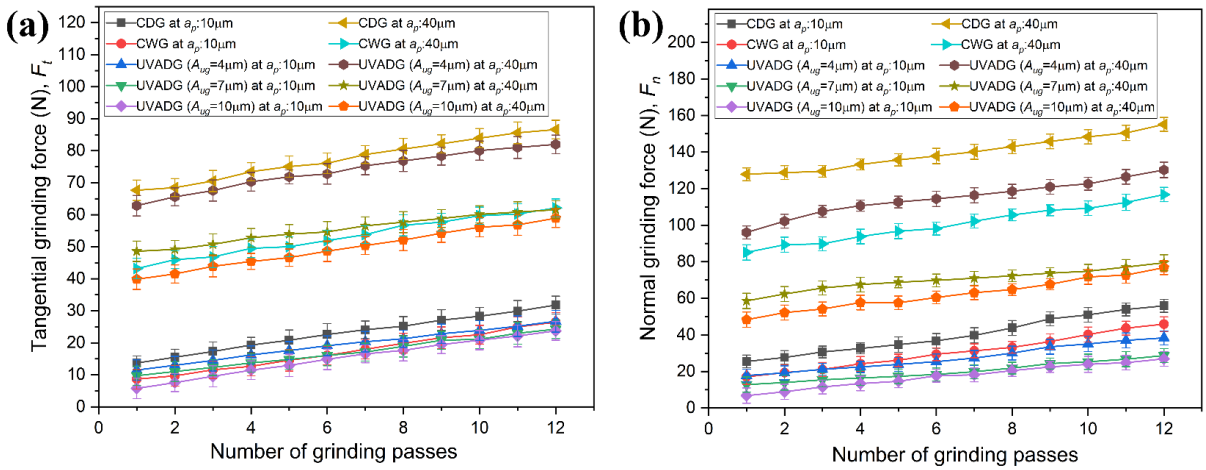

Figure 5.1 Variation of grinding forces (a) Tangential (b) Normal, with number of passes at downfeed of 10 and 40 µm under different modes

The UVADG (at A_{ug} = 10µm) mode can reduce the F_t and F_n compared with CDG and CWG modes under the same conditions. In addition, both the grinding forces during CDG, CWG and UVADG modes increase along with the increasing grinding passes. This may be due to the wear out of the grinding wheel grits with the increase of the grinding passes. Ding et al. [98] found an increase in grinding force with a number of passes while ultrasonic vibration grinding of silicon carbide. Also, the grinding forces were higher with the rise in downfeed in all grinding modes. An increase in downfeed at constant wheel speed led to increased maximum uncut chip thickness or wheel loading because of the increased friction between the abrasive wheel and ground surface interface. In case of UVADG, the material removal mechanism is varied due to the characteristic of separability. The cutting process becomes discontinuous because of the high-frequency interaction between active abrasive

grits and the ground surface. Therefore, the grinding forces increase relatively slowly during UVADG (A_{ug} = 10μm) with increasing the number of grinding passes compared with CDG and CWG modes. As presented in Figure 5.1 (a, b), during the first pass, the F_t obtained in UVADG (A_{ug} = 10 μm) mode was decreased by 41.06%, 13.26%, 26.56%, and 17.96% as compared to CDG, CWG, UVADG (A_{ug} = 4 μm), and UVADG (A_{ug} = 7 μm) modes, and F_n was reduced by 62.23%, 43.28%, 49.73%, and 17.62% as compared to CDG, CWG, UVADG (A_{ug} = 4 μm), and UVADG (A_{ug} = 7 μm) modes, respectively. While during the 12th pass, the F_t and F_n increased to 31.97% and 50.51% in CDG mode, 8.54% and 34.25% in CWG mode, 28.12% and 41.06% in UVADG (A_{ug} = 4 μm), and 4.31% and 3.34% in UVADG (A_{ug} = 7 μm) as compared to UVADG (A_{ug} = 10 μm) mode. As a result, it can be concluded that adopting UVADG modes makes it considerably easier to keep the grinding wheel sharp.

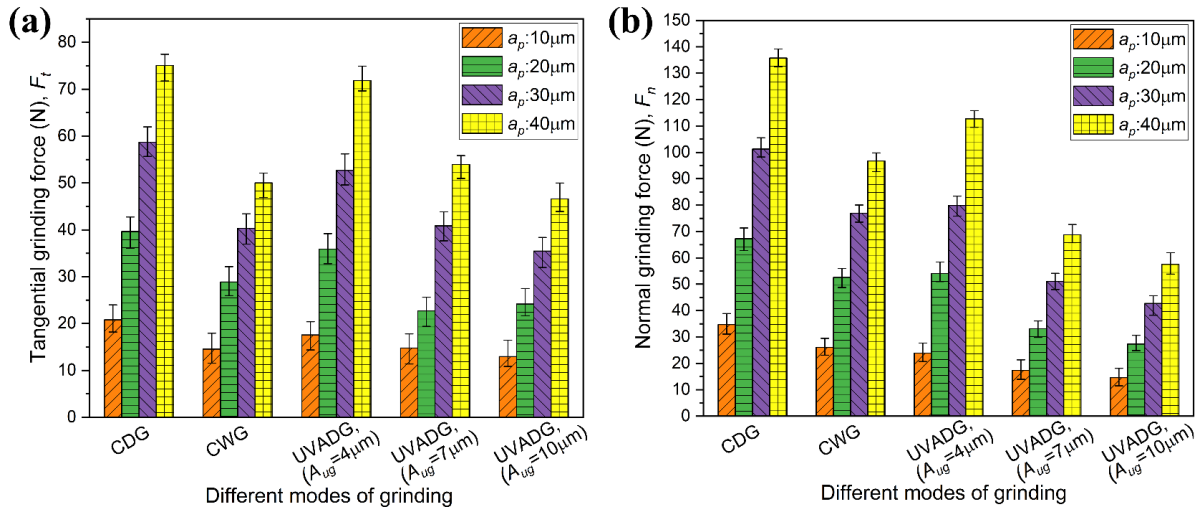

Figure 5.2 Variation of grinding forces (a) Tangential (b) Normal under different modes

The standard deviation of ground forces is illustrated by the error bar. Figure 5.2 depicts the grinding forces under CDG, CWG and UVADG (at A_{ug} = 4, 7, 10 μm) modes at downfeed of 10, 20, 30 and 40 μm, respectively, while worktable feed rate was 9 m/min. The grinding forces were computed without the forces for the first five passes to skip the

inconsistencies involved with eliminating the relative stiffness. The normal component of grinding force denotes the ease with which material can be removed due to abrasive penetration on the substrate surface. On the other hand, the tangential component denotes the ease with which material can be removed during shearing action, which is preferred to be the better effective reason for material removal. As shown in Figure 5.2 (a, b), the lowest F_t and F_n were found under UVADG (at A_{ug} = 10 μm) at respective downfeed with corresponding CDG and CWG modes. In the case of CDG mode, because of the ploughing and rubbing action of the abrasive wheel on the workpiece surface (refer to Figure 5.8) in the absence of coolant and lubrication, larger grinding forces (F_t and F_n) were generated in the machining zone. While the coolant in the CWG mode can advance toward the elastic grinding region, it is hard to approach the plastic grinding region owing to the hydrodynamic boundary layer forming around the abrasive wheel's periphery [109]. As a result, the coolant has a cooling impact on a smaller area of the ground sample, which increases the grinding forces. In UVADG mode, on increasing the vibration amplitude from A_{ug} = 4 μm to A_{ug} = 10 μm, the more effective is the influence of the engaged abrasive grits on the ground sample. The grinding zone generates an effective interaction between abrasive grits and the sample surface due to the discontinuous kinematics of the cutting process in ultrasonic grinding, allowing the material to begin removing more effectively. Therefore, frictional impact (refer to Figure 5.3) and F_t and F_n are reduced, resulting in very little plastic deformation (refer to Figure 5.8) occurs in UVADG.

5.2.2 Force ratio

The grinding force ratio is an important parameter in finishing operations because it offers quantitative information about the productivity of the grinding process. The ratio of tangential to normal grinding force can be used to calculate the friction coefficient (μ) or

grinding force ratio. Due to its similarity to a coefficient of friction, the same symbol, μ, is used [266]:

$$\mu = \frac{F_t}{F_n}$$

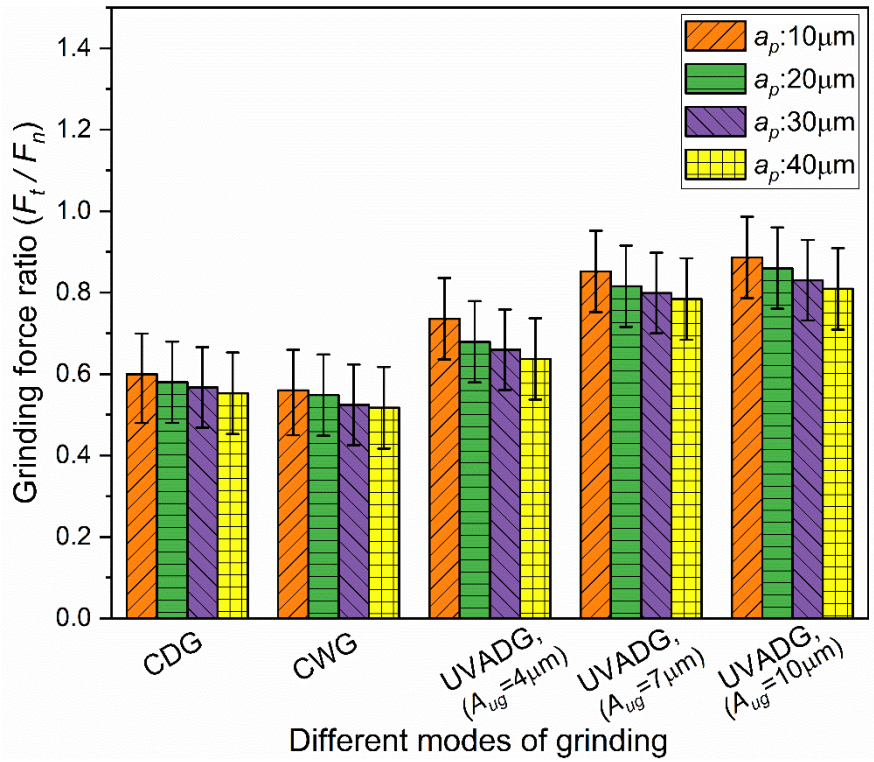

Figure 5.3 Variation of grinding force ratio in various grinding modes

Figure 5.3 shows the variation in the F_t/F_n ratio under the CDG, CWG, and UVADG (at A_{ug} = 4, 7, 10μm) modes at downfeed of 10, 20, 30 and 40 μm. As downfeed (a_p) increased, the corresponding F_t/F_n ratio was reduced in each distinct mode of grinding. The F_t/F_n ratio were seen to differ in the span of 0.5164 to 0.8863 under CDG (at a_p = 40 μm) and UVADG (at a_p = 10 μm), respectively. The F_t/F_n ratios in CWG, CDG, UVADG (at A_{ug} = 4 μm) and UVADG (at A_{ug} = 7 μm) grinding mode were 0.5164, 0.5531, 0.6357 and 0.7852, respectively, which were 35.12%, 32.43%, 22.29% and 4.10% smaller than that of UVADG (at A_{ug} = 10 μm). A high F_t/F_n ratio implies a sharper grinding wheel, while a low F_t/F_n

ratio means dull grinding wheel [267]. The UVADG mode provides a higher F_t/F_n ratio, indicating that the decrease in F_n was more significant than F_t. UVADG generates a self-sharpening tendency of the abrasive wheel to maintain the sharp edges of abrasive grits [268]. The sharp edges of abrasive grits caused more intense penetration into the work surface, reducing grinding forces.

5.2.3 Specific grinding energy

Specific grinding energy (e_c) gives a relevant measure of a grinding wheel's ability to withdraw material per unit volume. Figure 5.4 shows the graph between varying specific grinding energy with different modes of grinding under different equivalent chip thickness (h_{eq}), whereas h_{eq} is the thickness of the layer removed at each wheel speed and it is a measure of the material removal depth by the abrasive grits into the workpiece. A smaller value of specific grinding energy at same value of h_{eq} signifies that the efficiency of grinding mode is higher and less power consumption. Mathematically the equivalent chip thickness (h_{eq}) can be calculated from the equation (5.1) [8]:

$$h_{eq} = a_p \frac{V_w}{V_c} \tag{5.1}$$

Figure 5.4 illustrates the efficiency of different grinding processes. As presented in Figure 5.4, the highest e_c (27.33 J/mm^3) was obtained at 38.05nm h_{eq} under CDG because of the larger friction effect (grinding force ratio, refer to Figure 5.3) in the grinding region. The specific grinding energy of the CWG, UVADG at A_{ug} = 4 µm, UVADG at A_{ug} = 7 µm and UVADG at A_{ug} = 10 µm were 19.13, 23.1, 19.42, and 17.01 J/mm^3, respectively and which were 30.10%, 15.47%, 28.94%, and 37.76% lower than that of CDG. Specific grinding energy in the CWG was larger than UVADG at A_{ug} = 10 µm. In CWG with water-based soluble coolant as a cutting flood environment has inadequate lubrication in the cutting region and absorbs more energy in CWG mode than UVADG mode. In CWG mode, the

force ratio (coefficient of friction) and specific grinding energy are higher than UVADG mode, which clearly indicated that the coolant in the cutting zone was not ideal.

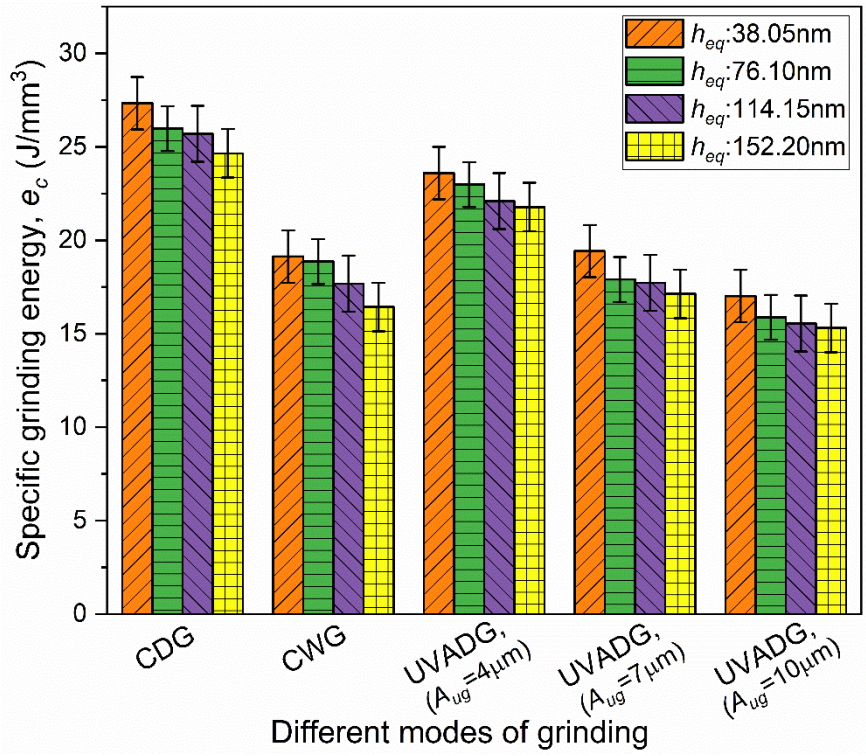

Figure 5.4 Specific grinding energy versus equivalent chip

This is due to a large-scale scattering of coolant flow, and the reason was due to a lower velocity of coolant in CWG mode. The hydrodynamic boundary layer throughout the periphery of an abrasive wheel may be formed due to the lower velocity of coolant for diffusion in the grinding region. Therefore, an improvement in the rubbing activity among grinding wheel and workpiece material followed in an increment in ground forces that used more specific grinding energy in CWG. It is clear from Figure 5.4 that UVADG efficiency is much higher than the efficiency of CDG and CWG. In UVADG, the specific grinding energy reduces with raising h_{eq}, this is owing to F_t in UVADG increases less than proportionately with h_{eq} and it is known as size effect. Rowe and Chen [269] described grinding performance by the size effect and bluntness of the abrasive wheel grits and further

explained the size effect using 'sliced bread analogy'. In addition to that, mathematically, the 'size effect' is defined by the equation ($e_c = F_1 * (h_{eq})^{n-1}$), where F_1 and n are the constant. Due to the value of the exponent of h_{eq} is negative, the relation in the above equation reveals the specific grinding energy increases when the equivalent chip thickness (h_{eq}) decreases. This phenomenon is the so-called size effect.

5.2.4 Surface Roughness

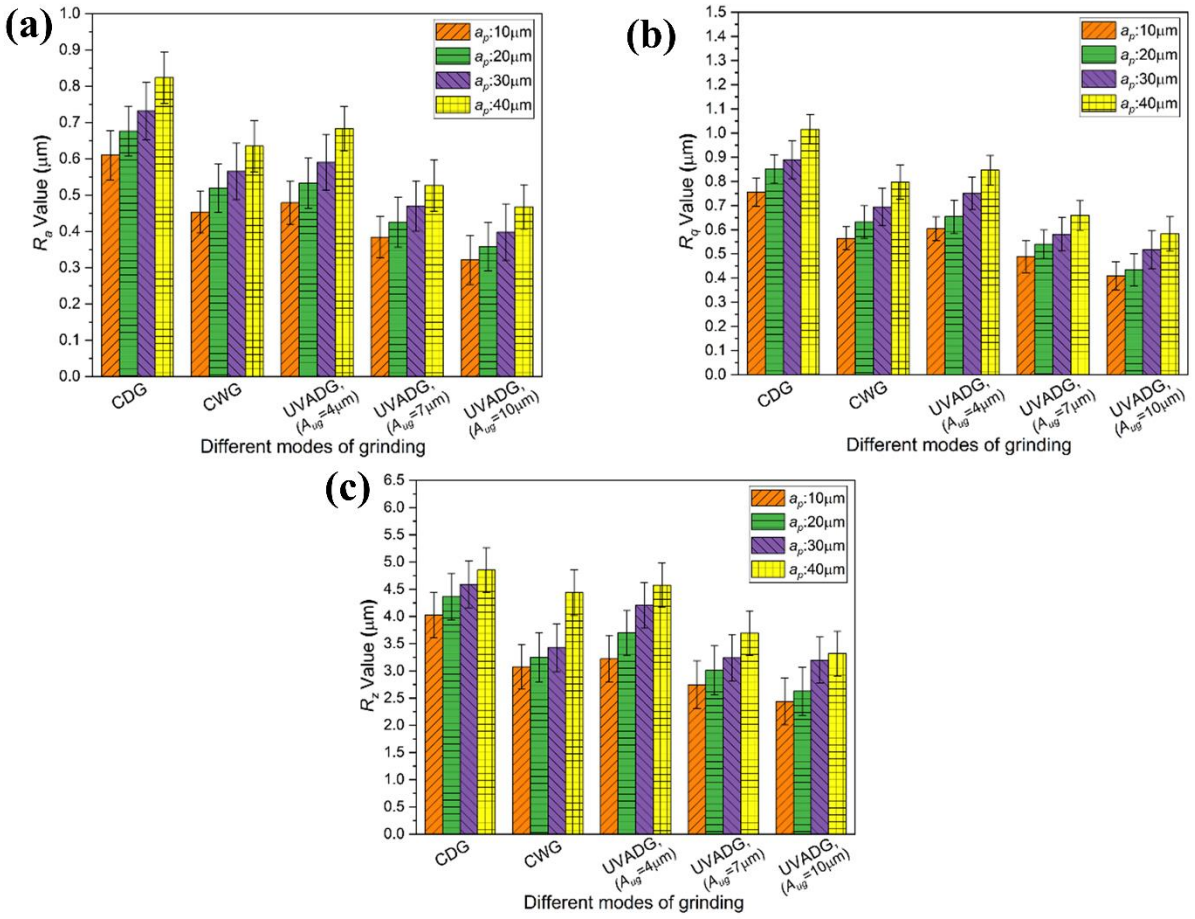

Figure 5.5 Variation of (a) R_a Value, (b) R_q value, (c) R_z value under different modes

Surface roughness is accountable for a substantial degree of the functional characteristics of ground surfaces. Therefore, a rational selection of parameters for surface roughness estimation is essential. Arithmetical mean height indicates the average of the absolute value

along the sampling length known as the arithmetical mean height of the surface roughness (R_a). Root mean square deviation indicates the root mean square along the sampling length known as root mean square (RMS: R_q).

The average maximum height of the profile indicates the absolute vertical distance between the five maximum profile peak height and the five maximum profile valley depth along the sampling length known as maximum height of profile of the surface roughness (R_z). The R_a, R_q, and R_z parameters are extensively used in precision manufacturing industries for period bearing area analysis, which provides qualitative information regarding wear resistance of ground sample [270]. Figure 5.5 (a, b, and c) depicts surface roughness (R_a, R_q, and R_z) of the ground workpiece under CDG, CWG and UVADG modes of grinding, respectively and surface roughness increased by increasing the a_p under each mode of grinding. Larger depth of cut followed in larger maximum uncut chip thickness, the reason behind that surface roughness is linearly related to maximum uncut chip thickness in grinding [271]. The highest R_a, R_q and R_z values 0.82µm, 1.02µm and 4.85µm were noticed in CDG, because of larger rubbing and ploughing effect as compared to CWG and UVADG (refer to Figure 5.8). The R_a values under CWG, UVADG at A_{ug} = 4 µm, UVADG at A_{ug} = 7 µm and UVADG at A_{ug} = 10 µm were 0.63µm, 0.68µm, 0.52µm and 0.46µm respectively, and which were decreased by 22.92%, 17.03%, 36.09% and 43.23% to that of CDG, respectively. The R_q values under CWG, UVADG at A_{ug} = 4 µm, UVADG at A_{ug} = 7 µm and UVADG at A_{ug} = 10 µm were 0.79 µm, 0.84 µm, 0.65 µm and 0.58 µm, respectively. These values decreased respectively by 21.42%, 16.63%, 35.03% and 42.59% to that of CDG, respectively. The R_z values under CWG, UVADG at A_{ug} = 4 µm, UVADG at A_{ug} = 7 µm and UVADG at A_{ug} = 10 µm were 4.43 µm, 4.57 µm, 3.69 µm and 3.21 µm respectively, and which were decreased by 8.56%, 5.73%, 23.91% and 33.69% to that of CDG, respectively. As shown in Figure 3.4 (c), the path of traditional grinding is linear

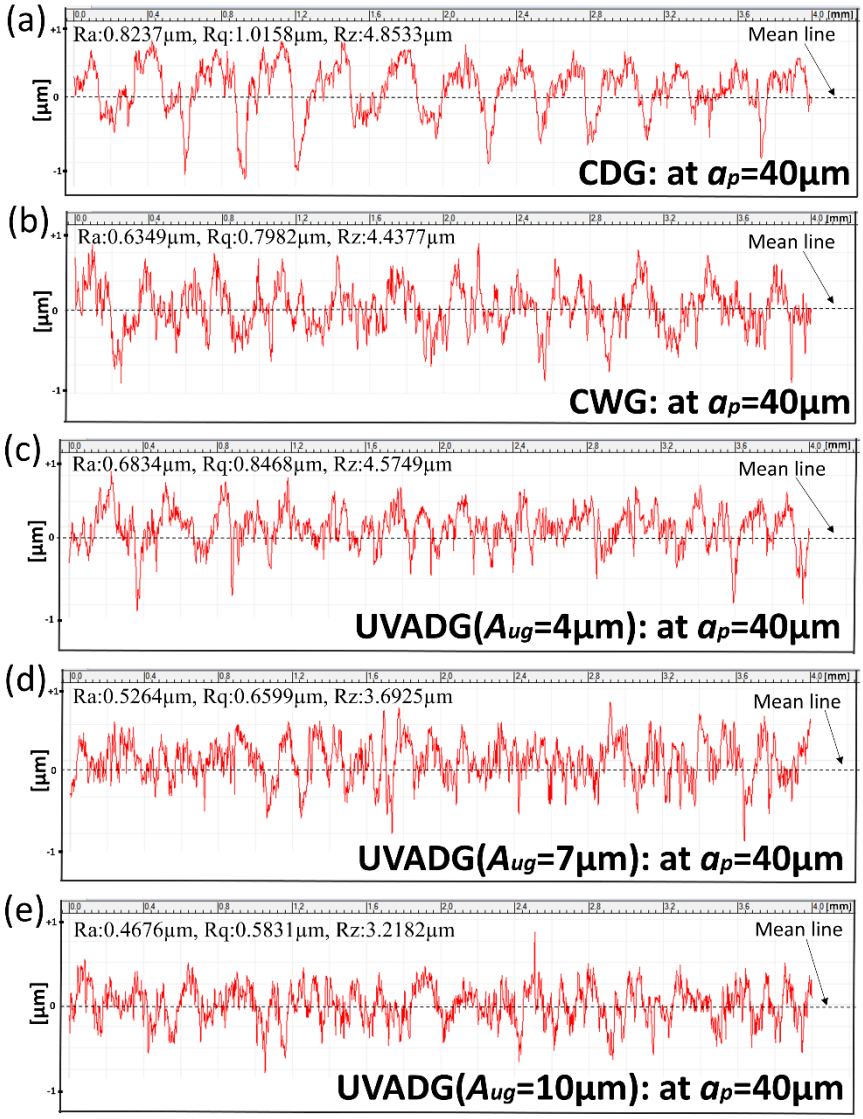

Figure 5.6 2D surface profile of the ground workpiece

while UVADG follows a sinusoidal path because of ultrasonic vibration amplitude on the workpiece surface. Therefore, the breadth ($2A_{ug}$) of the cutting groove in UVADG is presented in Figure 3.4 (c), which is broader than that in conventional grinding. Due to this, the wider grinding grooves and more regular grinding surfaces can be achieved.

Figure 5.6 shows the 2D profiles of the ground workpiece surface transverse to the grinding direction in CDG, CWG and UVADG with the downfeed, and worktable feed rate of 40 µm and 9 m/min respectively. It can be observed that the profile generated by CDG and

CWG (Figure 5.6 (a) and (b)) has spiky ribs, and the appearance of the profile points are approximately uniform around the mean line.

In contrast, the profile produced by UVADG has a comparatively flat tip, and the profile points are shifted to the bottom of the mean line. As the ultrasonic vibration amplitude increases (A_{ug} = 4 µm to A_{ug} = 10 µm), the smaller becomes the value of the peak-valley spacing as displayed in Figure 5.6 (c, d and e). This results in decline of the R_a, R_q and R_z values. Hence, after UVADG the surface roughness decreases significantly. As ultrasonic vibration assisted grinding utilizes supplementary stress to support in disintegrating the instantaneous welds, they decrease the time in the course of which any two asperities on counter surfaces may continue in temporary contact and, therefore, it prevents them from developing a stable weld [90]. This implies, in UVADG, a lesser amount of stable bonds among the abrasive grits and workpiece material surface is formed. Hence the surface roughness decreases in UVADG.

5.2.5 Bearing area characterises

The contact state of two physical surfaces is referred to as the bearing area curve (BAC), and it offers qualitative information on component wear resistance. The BAC indicates the percentage or linear fraction of a profile over a specific height. Surface roughness findings may be easier to understand if the BAC is divided into subsections, such as core roughness depth (S_k), reduced peak height (S_{pk}), and reduced valley depth (S_{vk}), which were calculated using the BAC based on the ISO 25178-2 (2012) standard [272], as shown in Figure 5.7 (c). A straight line based on a best-fit line across 40% of the BAC's centre part can be drawn for this purpose. Furthermore, the BAC ratio (SMr2-SMr1) is expressed as a percentage area encountered by intersecting a line that divides the peak and valley profiles from the core profile. In addition to that, the peak material portion (SMr1) specifies the percentage of material that includes the S_{pk} peak structures, and the valley material portion (SMr2)

refers to the percentage of the measurement area that constitutes the S_{vk} deeper valley structures. The higher BAC ratio showed that the machine parts had a larger bearing area and enhanced antifriction and antiwear characteristics [153]. This research examines the BAC of various ground workpieces for a qualitative surface quality assessment in different grinding modes. Figure 5.7 (a, b) illustrates the BAC and BAC ratio of the ground workpiece under CDG, CWG, and UVADG modes with varying ultrasonic vibration amplitude. In UVADG mode, a higher BAC ratio was achieved because of the impact of overlapping induced by ultrasonic vibration. The higher ultrasonic amplitude (at A_{ug} = 7 and 10 µm) can induce better evident overlapping. This might be the reason that an increase in the ultrasonic vibration amplitude generated a higher BAC ratio, which considerably prevents the rubbing activity on the ground surface.

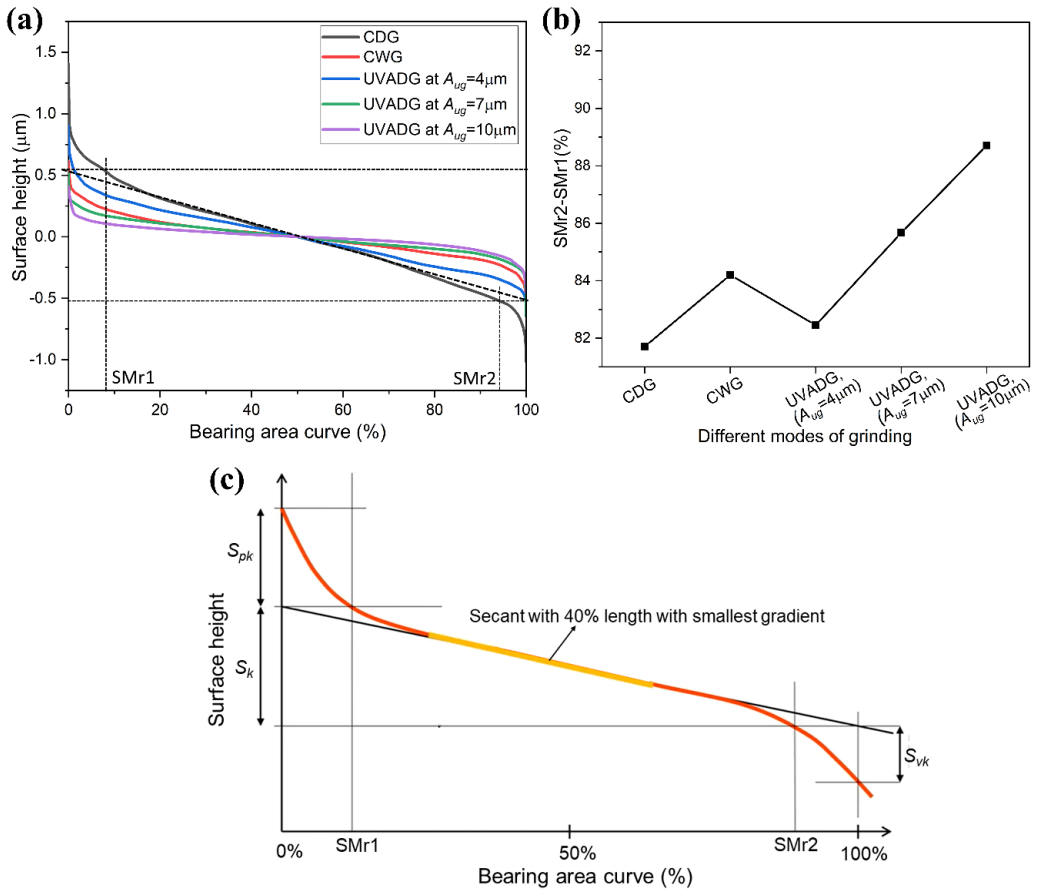

Figure 5.7 Bearing area assessment under various grinding modes: (a) Bearing area curve (b) Bearing area curve ratio (c) Parameters of bearing area curve

To put it another way, the core roughness profile generated a steeper BAC. The CWG mode has a nearly identical BAC shape to the UVADG mode (at A_{ug} = 7 μm) but a slightly lower BAC ratio (refer to Figure 5.7 (a, b)) due to multiple valley points on the ground surface that affect the entire BAC. The CDG mode had the lowest BAC ratio, revealing relatively deep scratches on the ground surface due to the lack of coolant. In addition to that the reduced peak height S_{pk}, the parameter illustrating the height at which peaks rise from the core profiles, gives information about the running-in process of the surface. A lower S_{pk} value corresponds to a shorter running-in phase and provides more initial contact area, therefore, lower area of contact stress when contact occur between the wheel and workpiece [150] [273]. As shown in Figure 5.7 (a) and Table 5.2 Parameter of Bearing area curve, the S_{pk} value of UVADG (at A_{ug} = 10 μm) is lower than that of UVADG (at A_{ug} = 7 μm), CWG, UVADG (at A_{ug} = 4 μm), and CDG, respectively. That means the running-in time and area of contact stress of the ground surface after UVADG (at A_{ug} = 10 μm) is smaller than that after UVADG (at A_{ug} = 7 μm), CWG, UVADG (at A_{ug} = 4 μm), and CDG, respectively.

Table 5.2 Parameter of Bearing area curve

Mode	S_{pk} (μm)
CDG	1.41
CWG	0.62
UVADG (at A_{ug} = 4 μm)	0.90
UVADG (at A_{ug} = 7 μm)	0.51
UVADG (at A_{ug} = 10 μm)	0.43

Furthermore, the core roughness height of UVADG (at A_{ug} = 10 μm) is more centralized than that of UVADG (at A_{ug} = 7 μm), CWG, UVADG (at A_{ug} = 4 μm), and CDG, respectively. Hence, the core roughness depth S_k, which describes the part of the roughness profile without any peaks or valleys are shorter in UVADG (at A_{ug} = 10 μm) than that in UVADG (at A_{ug} = 7 μm), CWG, UVADG (at A_{ug} = 4 μm), and CDG, respectively. During

operation, there is high mechanical resistance, and hence, the manufacturing process is constructively controlled by providing lower S_k values [150] [273]. This signifies that the bearing capacity of the finished surface after UVADG (at A_{ug} = 10 μm) is best to that after UVADG (at A_{ug} = 7 μm), CWG, UVADG (at A_{ug} = 4 μm), and CDG, respectively.

5.2.6 SEM and AFM micrographs

Surface morphology and topography is a critical criterion for determining surface integrity. This index indicates the interaction of abrasive grits with the ground surface and material removal mechanism. The most efficient direct techniques for evaluating microscopic changes in finished parts are SEM and AFM. SEM (2D) and AFM (3D) micrographs of ground surface morphology and topography at 40μm downfeed under various grinding modes are shown in Figure 5.8. Deep grooves, severe ploughing, rubbing marks, and plastic deformation were noticed on the ground surface in CDG mode, as illustrated in Figure 5.8 (a). Also, excessive heat generation in the machining zone promotes the redeposition of the grinding material on the ground surface and compromises the surface quality of the finished component. This occurs due to prolonged abrasive grits contact with the workpiece surface, lacking a cooling and lubricating effect in CDG mode. Owing to the low thermal conductivity of workpiece material, grinding chips clung to the wheel's abrasive grits. Furthermore, those grinding chips were redeposited on the finished surface, resulting in ploughing, and rubbing marks on the ground component. In CWG mode, as illustrated in Figure 5.8 (b), minor rubbing and ploughing marks can be noticed on the ground surface owing to the insufficient strength of adsorption tribo-boundary films. However, the surface quality of the ground component was good as compared to CDG and UVADG (at A_{ug} = 4 μm) modes. On the other hand, UVADG mode produces smooth and uniform surfaces, as shown in Figure 5.8 (d, e). During UVADG mode, the workpiece surface separates from the abrasive grit within per cycle of ultrasonic vibration. Such discontinuous contact

reduces the total time for heat conduction between the workpiece and abrasive grits. This decreases the heat generated in the grinding zone and wheel wear, which eventually enhances the surface quality of the ground workpiece. In several industrial applications, the surfaces of the components interacted in three dimensions. A surface roughness assessment based on a two-dimensional technique may not correctly describe a surface. Surface roughness can be more precisely determined by measuring it over an area than a line [274]. The surface parameters indicated using a three-dimensional method are shown by *S* instead of *R*. According to the AFM findings, as shown in Figure 5.8, the arithmetic mean height surface roughness (S_a) value of the ground workpiece at 40µm downfeed under CDG, CWG, UVADG (at A_{ug} = 4µm), UVADG (at A_{ug} = 7 µm) and UVADG (at A_{ug} = 10 µm) were 520.32, 403, 454.21, 311 and 202.1 nm, respectively. The total height surface roughness (S_t) value of the ground workpiece at 40 µm downfeed under CDG, CWG, UVADG (at A_{ug} = 4 µm), UVADG (at A_{ug} = 7 µm) and UVADG (at A_{ug} = 10 µm) were 3853, 2264, 2861, 2182 and 1486 nm, respectively. These outcomes confirmed that ultrasonic vibration provided better surface roughness (refer to Figure 5.7 (d, e)).

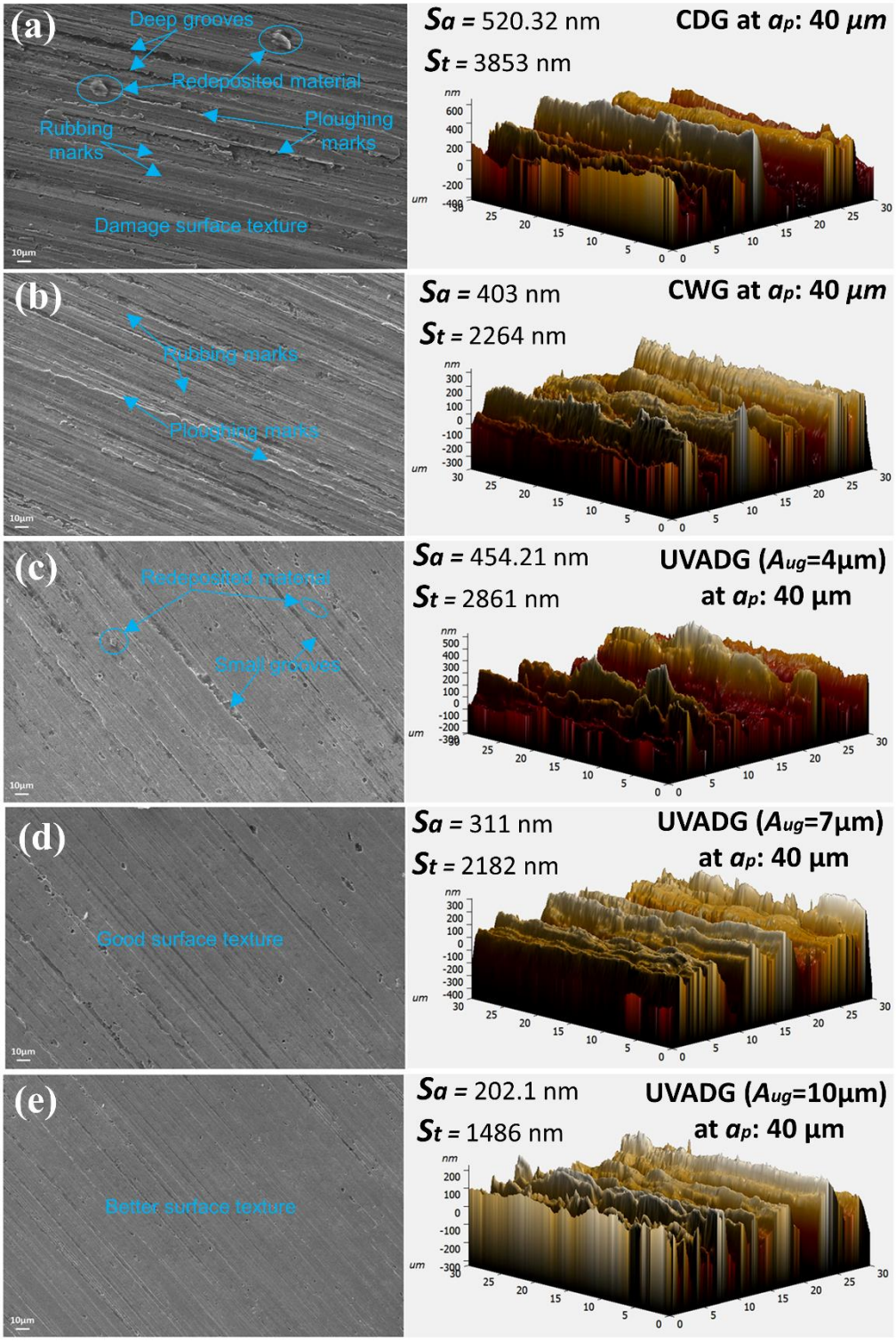

Figure 5.8 SEM (2D) and AFM (3D) micrographs of ground surface morphology and topography under various grinding modes (a) CDG, (b) CWG, (c) UVADG (A_{ug} = 4 μm), (d) UVADG (A_{ug} = 7 μm), (e) UVADG (A_{ug} = 10 μm)

5.2.7 Grinding temperature and grinding chip morphology

During the grinding process, the temperature is a crucial factor that affects the quality of the ground surface. The formation of microchip phenomena, such as rubbing, ploughing, and shearing action between the work material, grinding wheel, and nascent debris surfaces, significantly influences the grinding temperature. The underlying mechanism is also dependent on various grinding process parameters. Figure 5.9 (f) illustrates that an increase in downfeed leads to an increase in grinding temperature under all conditions. This is due to the increase in maximum uncut thickness. Unfortunately, the excess heat generated during grinding transfers to the work material, causing thermal damage and uneven cracks on the ground surface. Previous research has found that the surface quality of the ground sample deteriorates with more heat penetration. Figure 5.9 (a-e) presents, infrared thermographic grinding temperature profile under various grinding modes at highest downfeed 40 μm, and Figure 5.9 (f) shows the relation between the grinding temperature and various grinding modes at different downfeed. As shown in Figure 5.9 (f), the downfeed increases from 10 to 40 μm, the CDG mode grinding temperature increases from 390 to 647°C, the CWG mode grinding temperature increases from 324 to 449°C, the UVADG (at A_{ug} = 4 μm) mode grinding temperature increases from 387 to 643°C, the UVADG (at A_{ug} = 7 μm) mode grinding temperature increases from 322 to 451°C, and the UVADG (at A_{ug} = 10 μm) mode grinding temperature increases from 291 to 412°C. When compared to the CDG and CWG modes, the grinding temperature of the UVADG (at A_{ug} = 10 μm) mode is typically lower, decreasing by 25.38 to 36.32% and 10.18 to 8.24%, respectively. The grinding temperature reduces with the increase of vibration amplitude, as illustrated in Figure 5.9 (c-f).

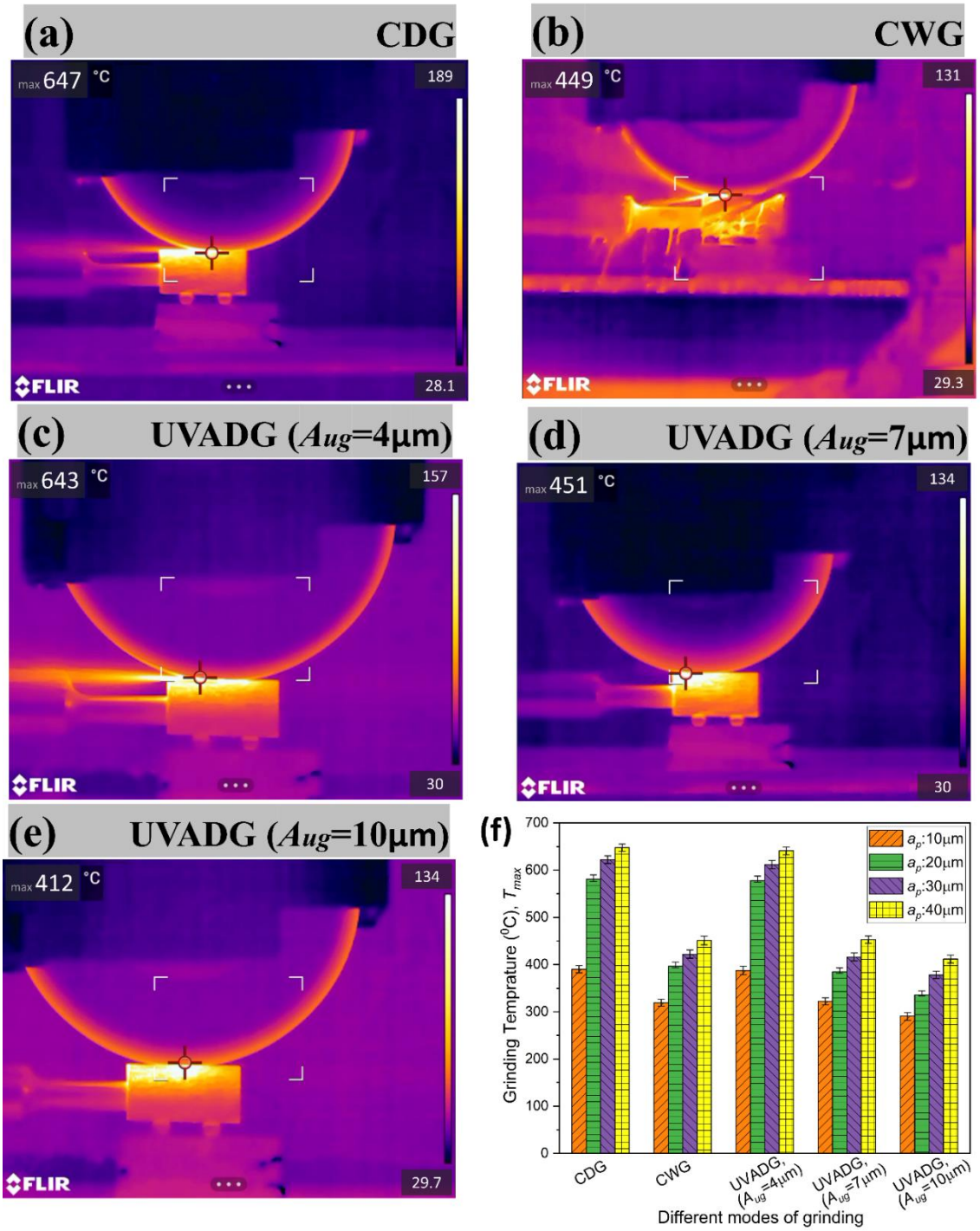

Figure 5.9 (a-e) Infrared thermographic grinding temperature profile under various grinding modes at a_p = 40 µm, (f) Variation in grinding temperature under different modes at different a_p

The maximum grinding temperature of UVADG (at A_{ug} = 4 μm) was 643℃, and UVADG (at A_{ug} = 7 μm) was 451℃, which were decreased by 35.92% and 8.64%, as compared to UVADG (at A_{ug} = 10 μm), respectively. This phenomenon demonstrates that by using ultrasonic vibrating methods in the CDG and CWG modes, the grinding temperature can be efficiently decreased because of within one ultrasonic vibration cycle while operating in UVADG mode, the workpiece surface separated from the abrasive wheel. The overall period for thermal conduction between the workpiece and abrasive wheel is shortened by such intermittent engagement. Therefore, effectively cooled the grinding zone by convective heat transfer to the surrounding environment. Consequently, a reducing grinding temperature pattern was seen during UVADG (at A_{ug} = 10 μm) mode, followed by CWG and CDG modes.

In order to maintain the effectiveness of the abrasive wheel or the ground surface throughout the grinding operation, grinding chip generation is a significant concern. Additionally, it offers qualitative information on the grinding burn that occurs while grinding. Figure 5.10 illustrates the morphology of grinding chips in different grinding modes. Grinding chips are produced because of the rubbing, ploughing, and shearing action of the abrasive wheel on the workpiece. Because of the lower thermal conductivity of AISI D2 tool steel, it performs poorly in heat transmission during machining. As a result, a large quantity of heat was generated on the ground surface, and the workpiece became thermoplastic in an imbalanced state. As shown in Figure 5.10 (a), during CDG mode, the long continuous and spherical chips were formed. Side flow/ploughing causes this sort of wider chip, which also entails significantly higher grinding forces (see Figure 5.2 (a-b)). Some irregularly shaped chips were also noticed under CDG mode, which is caused by the rubbing action that occurs between the workpiece surface and the abrasive wheel grit. Due

to the absence of coolant in CDG mode, this immense heat is sometimes not promptly transmitted from the grinding zone, resulting in the entire melting of grinding chips.

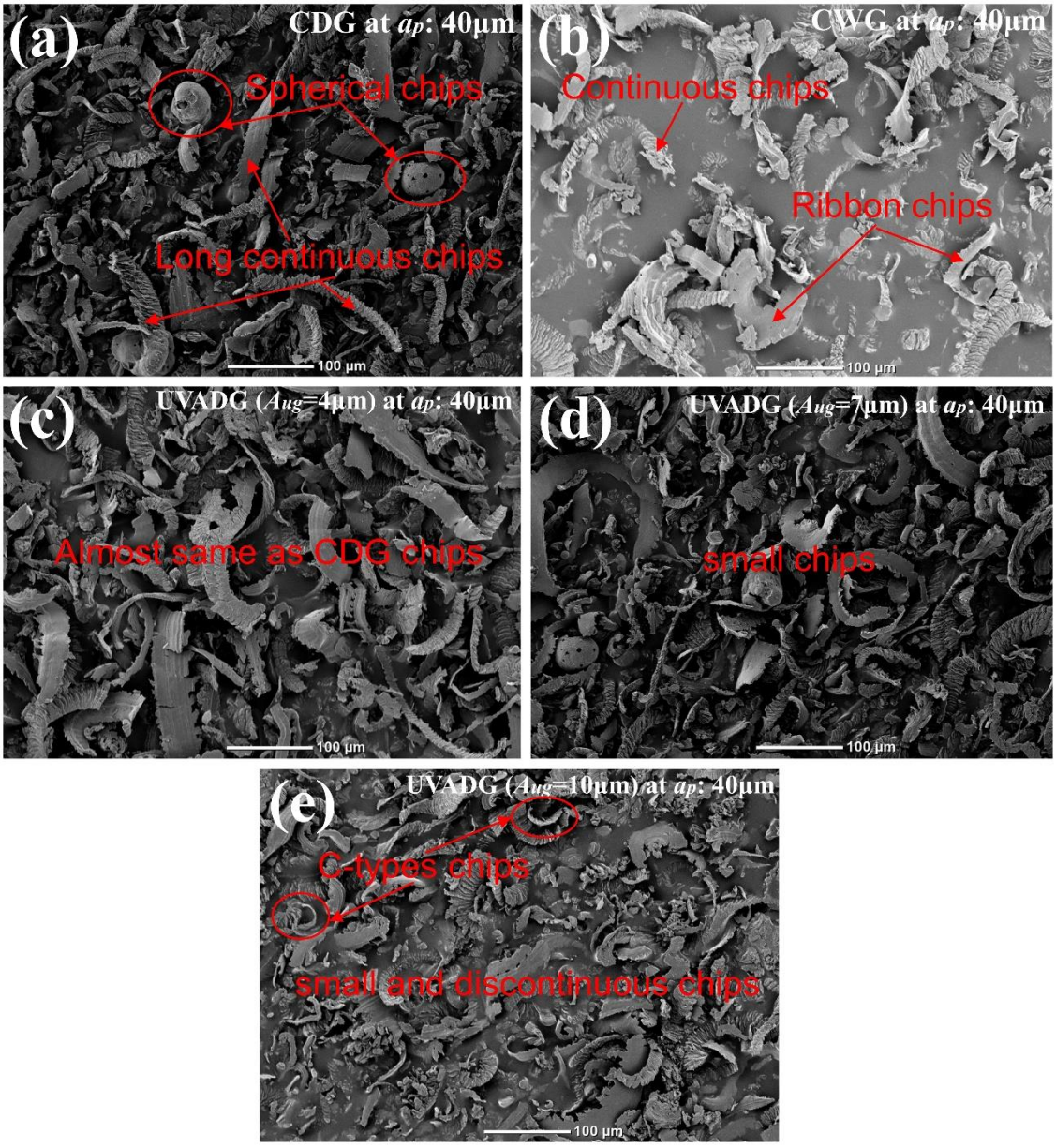

Figure 5.10 Grinding chip morphology under various grinding modes

It is transformed into a spherical form, and it is due to the larger oxidation and surface tension effects that generate this behaviour [257]. The chips formed under CWG mode were moderate in structure, as illustrated in Figure 5.10 (b). The CWG mode generated smaller

continuous and ribbon-type chips than the CDG mode, presumably owing to the action of cutting fluid. As shown in Figure 5.10 (c-e), the ultrasonic vibration amplitude increases from A_{ug} = 4 µm to A_{ug} = 10 µm resulted in smaller grinding chips. However, as shown in Figure 5.10 (e) the UVADG (at A_{ug} = 10 µm) mode has worked significantly, which can be demonstrated by the small discontinuous chips, C-type chips, and thinner chips. Ideal chips like this are often generated through shearing action, which requires less force. The reduced grinding forces achieved during the UVADG (at A_{ug} = 10 µm) mode (refer to Figure 5.2 (a-d)) further demonstrate that this is the most appropriate method of grinding.

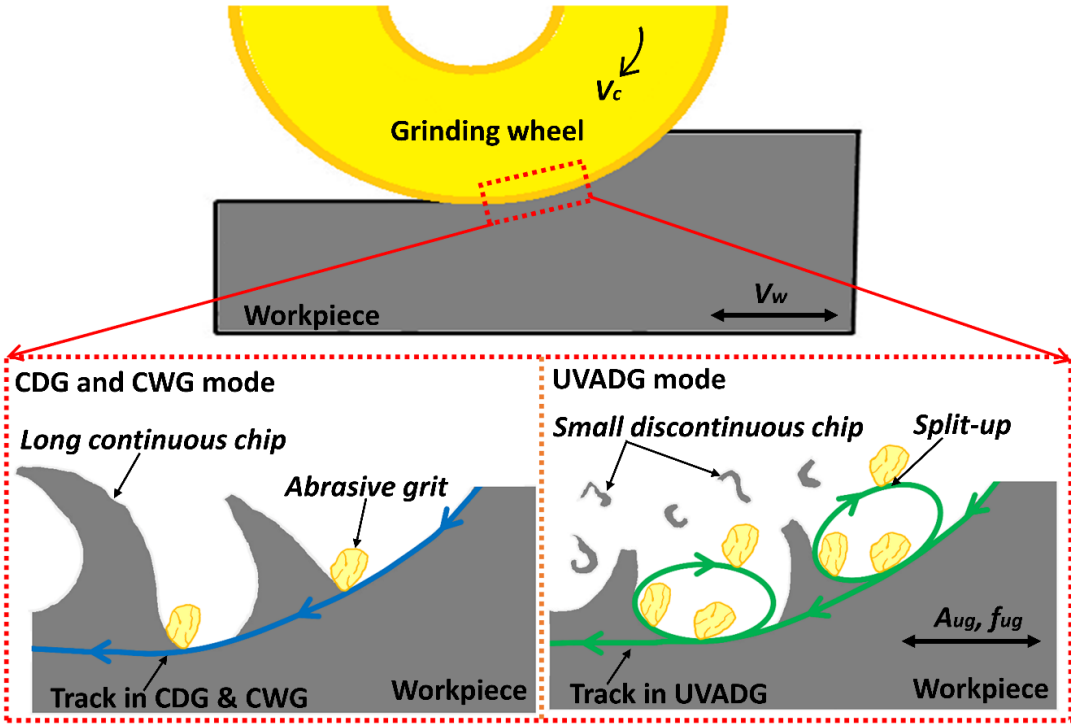

Figure 5.11 Representation of conventional grinding and UVADG mode grinding chip formation characteristics

Figure 5.11 represents the grinding chip formation characteristics of the conventional grinding and UVADG modes. When grinding hard-to-machine materials, the long continuous grinding chips usually appear when the downfeed is high. When compared to UVADG mode, conventional grinding shows a continuous linear cutting tack of abrasive grit particles. Furthermore, in the case of the conventional grinding mode, the grinding

chips were broader and larger than those in the UVADG mode. In the case of UVADG mode, the cutting track alters, and a split-up stage occurs between the abrasive grit particles and the workpiece. In UVADG mode, the matching long continuous grinding chips were split into short discontinuous grinding chips with thinner, short morphologies. In certain ways, the separating characteristics of UVADG mode enable chip breakdown. The analysis of grinding chip morphology demonstrates that the UVADG mode has the ability to improve the grinding performance of AISI D2 tool steel.

5.2.8 Microstructure and microhardness analysis

Figure 5.12 presents optical micrographs of the ground sub-surfaces cut perpendicular to the grinding direction under different grinding modes. From optical micrograph, it was observed that the CDG ground sample had experienced maximum thermal damage, while the UVADG (A_{ug} =10µm) surface encountered almost negligible thermal damage. Generally, the F_n has the greatest influence on the plastic deformation and roughness of the ground surface, while the F_t affects heat formation in the grinding zone[86]. As present in Figure 5.2, the UVADG (A_{ug} = 10 µm) has lower $F_{n,}$ and F_t as compared to CDG and CWG. Therefore, less heat was generated in UVADG (A_{ug} = 10 µm) as compared to that in conventional grinding. During grinding, a vast amount of heat generated in the grinding region due to the high negative rake angle of the arbitrarily orientated abrasive grits rubbing on the workpiece material. A significant part of heat was carried away by the grinding chip. Some part of the heat penetrated inside the top surface and subsurface of workpiece material, which influences the ground component's microstructure and mechanical properties.

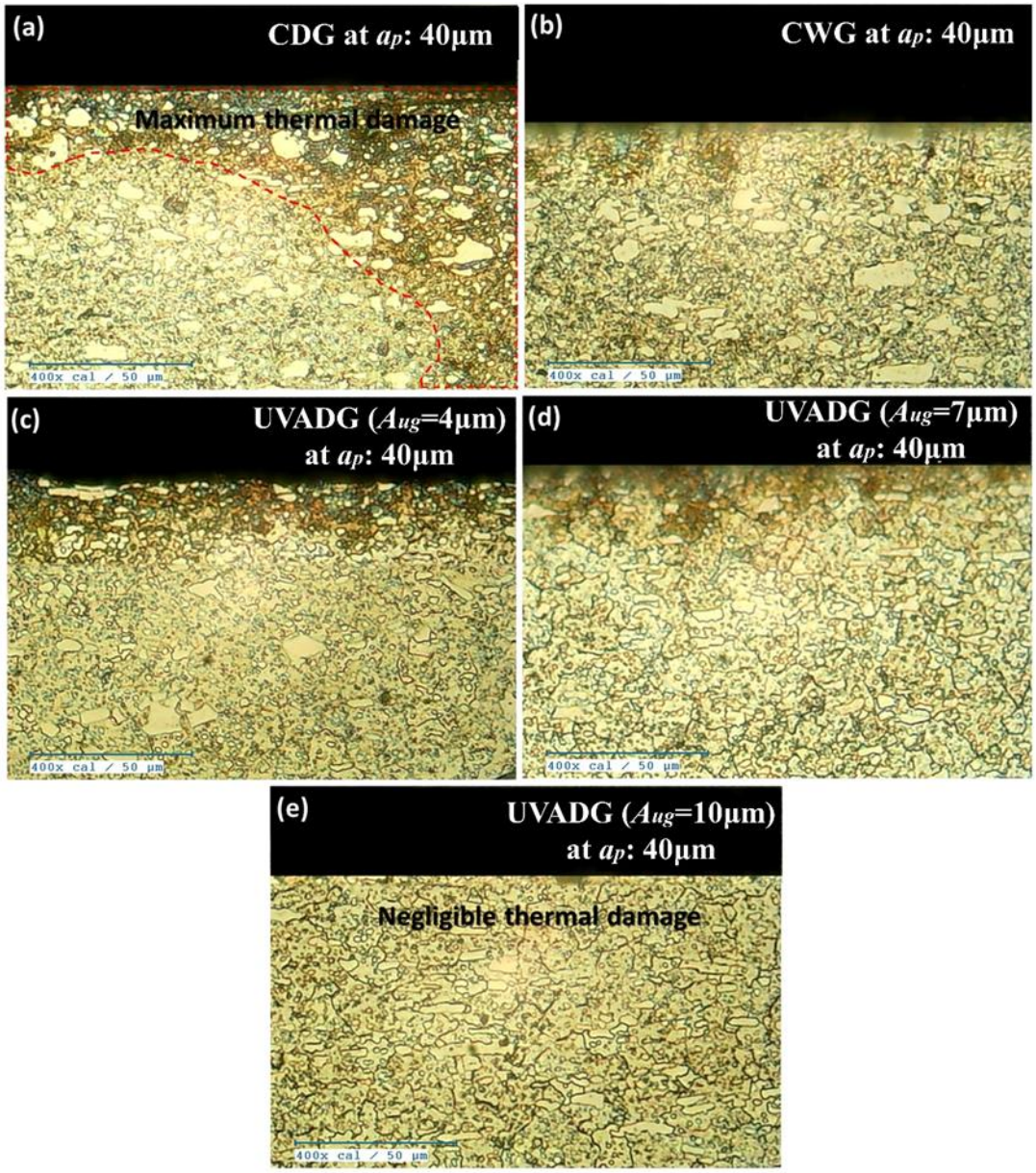

Figure 5.12 Optical microstructure micrograph of the cross-section of ground surfaces under different grinding modes

Therefore, microhardness estimation of the ground workpiece surface is necessary from the surface integrity perspective. The change in hardness of the top surface of workpiece under CDG, CWG, and UVADG mode was reported in Figure 5.13. High grinding zone temperature followed by rapid cooling induces varying degree of plastic deformation in the subsurface and thereby alters the microhardness of the ground sample. Commonly,

increased chip thickness and chip load during grinding results into larger plastic deformation on the surface and subsurface causing work hardening. This increase in hardness of the ground surface is undesirable as cracks can easily nucleate and propagate in the hard and brittle surface, leading to sudden failure of the ground component. Microhardness values observed under UVADG (at A_{ug} = 10 µm) was least (684 HV) as compared to those in CWG (801 HV) and CDG (849 HV) conditions.

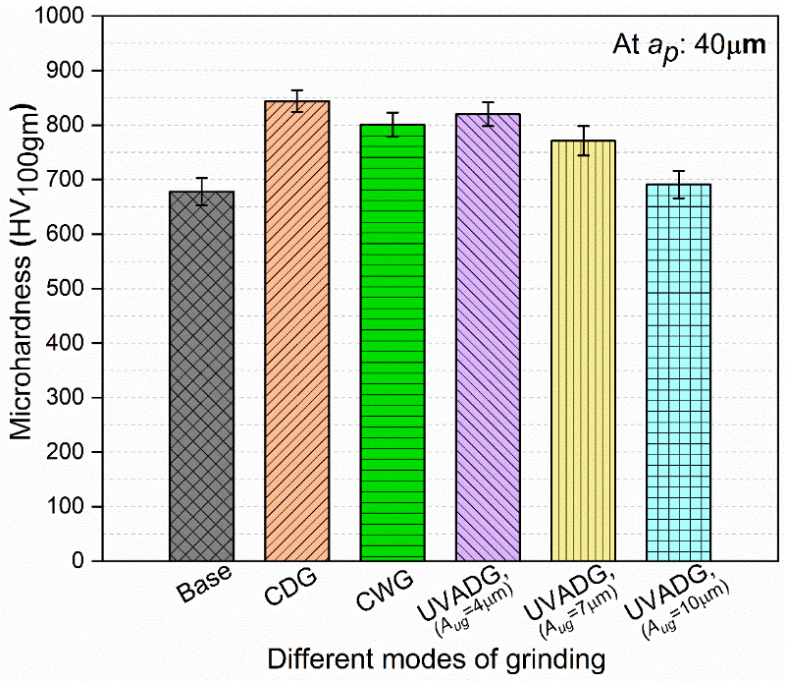

Figure 5.13 Microhardness on top of the ground surface under different grinding modes

However, microhardness of the base sample was 677 HV. The higher microhardness in the case of CDG may be attributed to the higher grinding zone temperature. This phenomenon produces more serious thermal damage in the absence of cutting fluid. Whereas in UVADG, discontinuous cutting action, less plastic deformation and lower frictional effects decrease the hardness of the ground sample.

5.2.9 Conclusion

In this experimental research work, ultrasonic vibration was implemented in the grinding of AISI D2 tool steel to illustrate the benefits of UVADG. The grinding performance was thoroughly investigated, including the grinding force and force ratio, specific grinding energy surface roughness, bearing area curves, ground surface quality, grinding temperature, chip morphology, microstructure, and microhardness. The following is a summary of the key conclusions:

- In terms of grinding forces, ultrasonic vibration (at A_{ug} = 10 µm) in the UVADG mode was effective in significantly decreasing grinding forces compared to CDG and CWG modes due to their intermittent cutting activity and very little plastic deformation, and smaller frictional effect.
- Because of UVADG mode grinding wheels self-sharpen, the grinding force ratio was greater than in CDG and CWG modes. A greater force ratio denotes a sharper grinding wheel, whereas a lower ratio denotes a dull grinding wheel.
- The efficiency of UVADG at A_{ug} = 10 µm was higher than CDG and CWG at each equivalent chip thickness. The specific grinding energy of UVADG at A_{ug} = 10 µm, CWG, and CDG was 17.01 J/mm^3, 19.13 J/mm^3, and 27.33 J/mm^3, respectively. In UVADG, the specific grinding energy was reduced with raising in equivalent chip thickness; this was owing to the size effect.
- The surface roughness in UVADG (at A_{ug} = 7, and 10 µm) was lower than in CDG and CWG at each downfeed. The reduction in surface roughness parameters (R_a, R_q, and R_z) in UVADG (at A_{ug} = 10 µm) was 43.23%, 42.59%, and 33.69%, respectively, in comparison to CDG and 26.35%, 26.94%, and 27.48%, respectively, in comparison to CWG. The surface topography generated under UVADG has a comparatively flat tip,

and the profile points shifted to the bottom of the mean line. This resulted in a reduction in surface roughness in the UVADG mode.

- Ultrasonic vibration-induced overlapping resulted in a higher BAC ratio (88.71%) and a steeper BAC in UVADG mode (at A_{ug} = 10 μm). This BAC ratio represents the ground surface under UVADG mode, which has significant antifriction and antiwear characteristics.
- Compared to CDG and CWG modes, UVADG mode has provided smooth and uniform surfaces by separating the workpiece surface from the abrasive wheel during ultrasonic vibration cycles, improving ground surface quality.
- The UVADG (at A_{ug} = 10 μm) mode, followed by CWG and CDG modes under the same grinding parameters, produced the lowest grinding temperature. This is due to the short contact time between the grinding wheel grits and workpiece and cools the grinding zone through convective heat transfer to the surrounding environment.
- The small discontinuous and thinner chips formed under UVADG (at A_{ug} = 10 μm) mode show the easiness in grinding and the lesser force needed while grinding AISI D2 tool steel. Besides, C-type chips indicate that the separation characteristic of the UVADG (at A_{ug} = 10 μm) mode appropriately achieves chip breaking.
- It was observed that CDG ground sample had suffered the maximum thermal damage because of high heat generation and more intense transfer of heat into the ground surface, and UVADG (at A_{ug} = 10 μm) encountered almost negligible thermal damage due to less heat generation.
- No notable change in hardness was seen under UVADG (at A_{ug} = 10 μm). This was due to minimum plastic deformation in the ground surface under UVADG (A_{ug} = 10 μm) as compared to conventional grinding.